Effect of non-ideal clamping shape on the resonance frequencies of silicon nanocantilevers

2011 Nanotechnology 22 245501

(http://iopscience.iop.org/0957-4484/22/24/245501)

Nanotechnology **22** (2011) 245501 (9pp) doi:10.1088/0957-4484/22/24/245501

Effect of non-ideal clamping shape on the resonance frequencies of silicon nanocantilevers

Samuel Guillon[1,2], Daisuke Saya[1,2], Laurent Mazenq[1,2], Sorin Perisanu[3], Pascal Vincent[3], Arnaud Lazarus[4], Olivier Thomas[4] and Liviu Nicu[1,2]

[1] CNRS, LAAS, 7 Avenue du Colonel Roche, F-31077 Toulouse Cedex 4, France
[2] Université de Toulouse, UPS, INSA, INP, ISAE, UT1, UTM, LAAS, F-31077 Toulouse Cedex 4, France
[3] LPMCN, Université Claude Bernard Lyon 1 et CNRS, 43 boulevard du 11 novembre 1918, 69622 Villeurbanne Cedex, France
[4] Structural Mechanics and Coupled Systems Laboratory, Conservatoire National des Arts et Métiers, 2 rue Conté, 75003 Paris, France

E-mail: sguillon@laas.fr

Received 3 December 2010, in final form 22 March 2011
Published 20 April 2011
Online at stacks.iop.org/Nano/22/245501

Abstract
In this paper, we investigate the effects of non-ideal clamping shapes on the dynamic behavior of silicon nanocantilevers. We fabricated silicon nanocantilevers using silicon on insulator (SOI) wafers by employing stepper ultraviolet (UV) lithography, which permits a resolution of under 100 nm. The nanocantilevers were driven by electrostatic force inside a scanning electron microscope (SEM). Both lateral and out-of-plane resonance frequencies were visually detected with the SEM. Next, we discuss overhanging of the cantilever support and curvature at the clamping point in the silicon nanocantilevers, which generally arises in the fabrication process. We found that the fundamental out-of-plane frequency of a realistically clamped cantilever is always lower than that for a perfectly clamped cantilever, and depends on the cantilever width and the geometry of the clamping point structure. Using simulation with the finite-elements method, we demonstrate that this discrepancy is attributed to the particular geometry of the clamping point (non-zero joining curvatures and a flexible overhanging) that is obtained in the fabrication process. The influence of the material orthotropy is also investigated and is shown to be negligible.

(Some figures in this article are in colour only in the electronic version)

1. Introduction

The transition from the micro- to the nanoscale, or particularly from microelectromechanical systems (MEMS) to nanoelectromechanical systems (NEMS) arouses great interest in both science and technology [1]. The downscaling progress allows many benefits such as reduced size devices for large scale integration, higher performances, as in the case of mass detection, and decreased energy consumption.

Two main methods exist for the manufacture of nanosystems: the bottom-up approach, involving self-assembly building of nanosystems, and the top-down method, that uses micro- and nanofabrication processes to shape in the bulk material [1–11, 16–20]. The bottom-up method provides a relatively easy implementation and the ability to manufacture a large number of systems simultaneously; however, it is difficult and more or less random to manipulate the manufactured devices. With the top-down approach, systems are directly realized at the desired location.

Usually, the top-down approach uses optical lithography or electron beam lithography for structuring patterns on a substrate [1–11]. Conventional optical lithography, generally limited to micrometer resolution, does not allow high resolution for NEMS. In this context, we developed an optical

method for manufacturing NEMS, achieving resolutions below those of conventional lithography and even laser lithography. We used a UV stepper photo repeater (I Line CANON FPA 3000 i4/i5 NA 0.63) equipped with a strongly converging lens (i5) which drastically reduces the size of the insolated patterns. This method provides submicron size patterns while using photoresists which are less sensitive to the electron emissions frequently occurring in NEMS manufacturing processes.

The methods of characterization of NEMS are numerous, depending on the manufacturing process. Excitation and detection may be thermoelastic, piezoresistive [11] or optical [2–5]. Excitation by field effect emission inside a scanning electron microscope (SEM) and visual detection of resonance frequencies by the SEM is often used as a characterization tool for bottom-up devices [12–15]. Davis and coworkers have already developed the excitation of top-down poly Si nanocantilevers by DC and AC electrostatic force and visual detection by optical microscope and SEM [16–18]. Here, the nanocantilever is driven by the electrostatic force approaching a tungsten nanotip by an *XYZ* positioner inside the SEM. The resonance frequencies are visually detected by the SEM.

In this paper, we describe the fabrication process of silicon nanocantilevers and their mechanical characterization by electrostatic force inside an SEM. The fundamental out-of-plane and in-plane resonance frequencies are measured and compared to the analytical theory of a perfectly clamped cantilever beam, showing discrepancies. Then, some finite-element numerical simulations are proposed to take into account the particular clamping point geometry and the material orthotropy.

2. Fabrication of the silicon nanocantilevers

Silicon on insulator (SOI) wafers were used as the starting material. The thickness of the top silicon layer was 340 nm with a 1 μm-thick buried SiO_2 layer on a 525 μm-thick silicon substrate. The buried SiO_2 layer (which is etched for releasing nanostructures) served as sacrificial layer.

As the lithography tool, a stepper photo repeater was employed to define the nanocantilevers' shapes. By regulating the photo repeater exposure power, a minimum width of 100 nm was achieved. As with any optical lithography equipment, the photo repeater allows the use of various types of photoresist for an adequate etching process. Moreover, the essential of the photo repeater is the ability to obtain precise alignment (better than 50 nm). After the photoresist development, the top silicon layer was vertically etched by reactive ion etching (RIE) until an intermediate SiO_2 layer appeared. Then the intermediate SiO_2 was etched by dipping the entire wafer into a buffered hydrofluoric acid (BHF) solution for liberation of the structures. In order to avoid irreversible collapse and subsequent substrate sticking of the nanostructures, the water used to rinse the wafers was progressively changed to ethanol which was evaporated by heating. The fabricated cantilevers with lengths varying from 1 to 14 μm, widths varying from 100 nm to 1 μm and thickness of 340 nm are shown in figure 1.

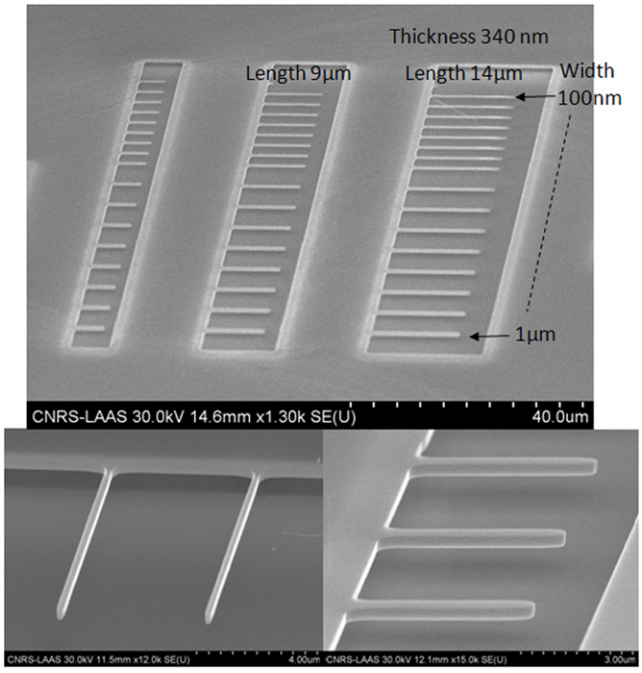

Figure 1. The silicon nanocantilevers of various sizes after liberation. The structures were defined by a stepper photo repeater (I Line CANON FPA 3000 i4/i5 NA 0.63).

3. Measurement of resonance frequency of the Si nanocantilevers inside an SEM

Excitation of cantilevers was performed individually via coupling between an AC voltage of a few volts brought near the apex by an etched tungsten tip and an induced electric charge on the cantilever. We induced a DC charge on the cantilever by adding a DC voltage of a few tens of volts to the excitation. The electric excitation force had thus a strong component at the excitation frequency. Each nanocantilever started vibrating when the frequency of the AC voltage matched its eigenfrequency. The resonances were detected by visual inspection on the SEM, by selecting the excitation frequency so that the motion amplitude was maximum. An *XYZ* nanomanipulator was used to bring the excitation tungsten tip to few tens of nanometers from the sample [12, 13] (figure 2). By this method of excitation and detection, both out-of-plane and in-plane resonances could be detected.

The main experimental challenge was to deal with the poor quality SEM image due to the applied AC voltage (see figure 3). Significant DC voltages had to be used in order to enhance the vibration amplitude for detection of the resonance frequencies. We obtained vibration amplitudes of the cantilever's end in the micron range, as shown in the out-of-plane and in-plane polarizations of the resonance in figure 3.

The eigenfrequencies of the nanocantilever series shown in figure 2 were measured and the results are given in table 1. The effective spring constant for the in-plane polarization increases with the width of the nanocantilever and thus makes visual detection in the SEM more difficult because of the lower amplitudes. That is the reason why values of in-plane frequencies with larger width are not included in table 1.

Table 1. Calculation and measurement results of the eigenfrequencies of the nanocantilevers with variation of width. Dimensions were measured by SEM observation.

Designed dimensions		Measured dimensions			In-plane eigenfrequency		Out-of-plane eigenfrequency	
Length (μm)	Width (nm)	Length (μm)	Width (nm)	Thickness (nm)	Calculated (MHz)	Measured (MHz)	Calculated (MHz)	Measured (MHz)
15	60	14.5	129	340	0.857	0.876	2.21	2.30
15	80	14.5	183	340	1.22	1.12	2.21	2.18
15	100	14.5	233	340	1.55	1.43	2.21	2.18
15	120	14.5	272	340	1.77	1.74	2.21	2.15
15	140	14.6	288	340	1.85	Not detected	2.18	2.13
15	160	14.6	325	340	2.08	Not detected	2.18	2.11
15	180	14.6	335	340	2.15	Not detected	2.18	2.10
15	200	14.6	421	340	2.70	Not detected	2.18	2.06
15	300	14.7	598	340	3.78	Not detected	2.15	2.04
15	400	14.7	743	340	4.70	Not detected	2.15	2.01
10	80	9.8	196	340	2.79	Not detected	4.84	4.91
10	100	9.8	235	340	3.34	3.24	4.84	4.89
10	120	9.8	279	340	3.97	3.86	4.84	4.79
10	140	9.8	316	340	4.50	4.31	4.84	4.78

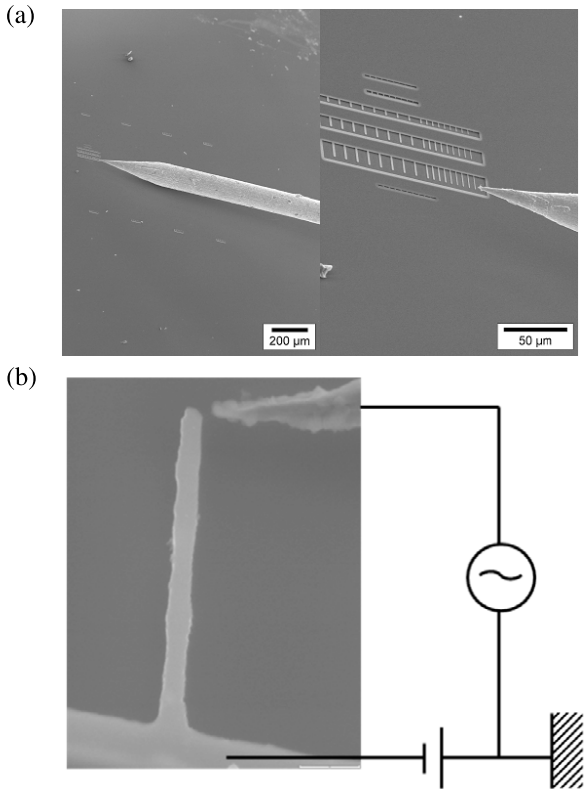

Figure 2. (a) Relative positioning of the tip and the sample, (b) excitation circuit.

Higher order modes were also difficult to observe. The charged apex of the cantilever moves in a varying electric potential which can affect the spring constant, the eigenfrequency and even induce nonlinear effects, as for an atomic force microscopy tip. We varied the distance between the excitation tip and the cantilever by more than a factor of two and we saw no measurable change in the mechanical eigenfrequencies. We concluded that the change was smaller than the natural Lorentzian width of the resonance, which determines the accuracy of our measurements.

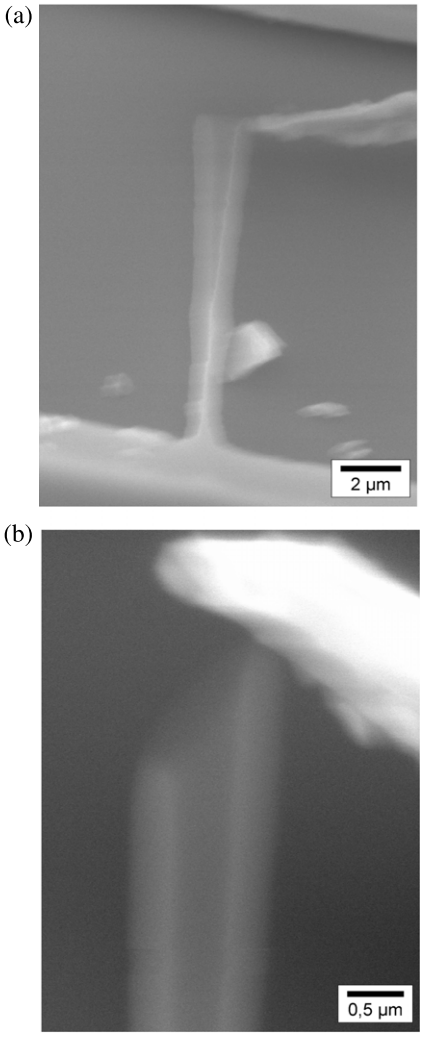

Figure 3. (a) In-plane and (b) out-of-plane resonance of a nanocantilever.

We saw nonlinear effects characterized by jumps and hysteresis for high excitation amplitudes. When we lowered the excitation amplitude, the jumps and hysteresis were no

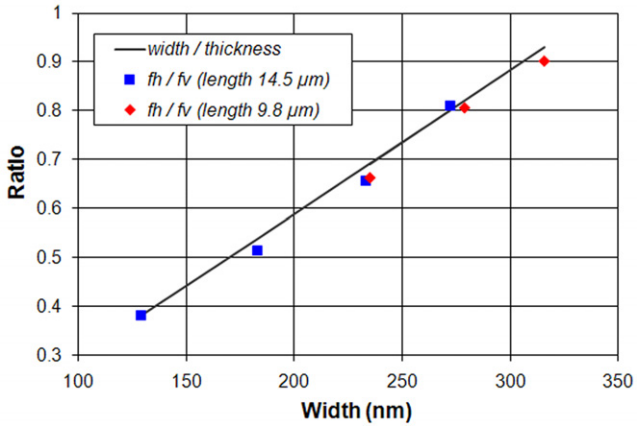

Figure 4. The ratio of in-plane frequency to out-of-plane frequency, f_h/f_v, and the ratio of width to thickness, b/e, as a function of the width b.

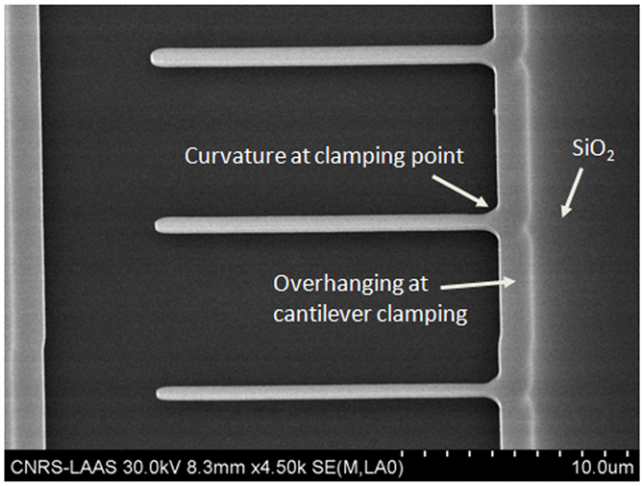

Figure 5. Top view SEM image of the nanocantilever. The SiO_2 layer is seen under the top Si layer due to the penetration of the electron beam. Curvature at the clamping point and overhanging at the cantilever clamping are also seen.

longer observable. This means that the nonlinearities change the eigenfrequency by less than the Lorentzian width given by the Q-factor ($\Delta f/f = 1/Q \approx 0.05\%$). Unfortunately, the quality of our SEM images was strongly affected by the electric potentials we used for the measurements and thus our curve of the response amplitude versus excitation frequency is not very accurate. For a cantilever beam, made of homogeneous material of Young's modulus E and density ρ and with a rectangular cross-section, the out-of-plane f_v (i.e. perpendicular to the wafer plane) and in-plane f_h (i.e. parallel to the wafer plane) eigenfrequencies are given by

$$f_v = \frac{\beta^2 e}{4\pi L^2}\sqrt{\frac{E}{3\rho}}, \qquad f_h = \frac{\beta^2 b}{4\pi L^2}\sqrt{\frac{E}{3\rho}} \tag{1}$$

where L, e and b denote respectively the length, the thickness and the width of the beam and $\beta = 1.875$ for the fundamental mode.

Relations (1) indicate that the in-plane resonance frequencies linearly increase with the width while not depending on the thickness; meanwhile, the reverse behavior is noted for the out-of-plane resonance frequencies.

The ratio of in-plane frequency to out-of-plane frequency, f_h/f_v, should always be equal to the width to thickness ratio, b/e, independently of any homogeneous variation of the material parameters. It is, for example, independent of the Young's modulus, and thus of the Si crystalline direction and also independent of the density. We can see that experimental data are in excellent agreement with this prediction in figure 4.

4. Discussion of the experimental data

The measured resonance frequencies are generally well consistent with calculation within a 10% error. Imperfection in measuring the dimensions in the SEM can explain the slight difference from the calculation.

It should be noted that, in the out-of-plane mode, the measured resonance frequencies decrease with the cantilever width value at supposedly constant length, contrary to the theoretical prediction (equation (1)). For instance, the out-of-plane resonant frequency of the 129 nm wide cantilever is 2.30 MHz while in the case of the 743 nm wide cantilever the out-of-plane resonant frequency value is 2.01 MHz. Due to the limitations in the precision of the photolithography technique, the measured length from one cantilever to another varies slightly. However this difference is limited to a few hundreds of nanometers which, according to the out-of-plane resonant frequency calculation using equation (1), cannot explain the decrease of the measured resonance frequency as can be seen in table 1. Hence, this must certainly be explained by non-ideal shapes of the fabricated nanocantilever structures.

One of these imperfections is the overhanging of the cantilever clamping point (see figure 5). The clamping zones of the cantilevers are subjected to undercut in releasing the cantilevers' structure by BHF etching of the SiO_2 sacrificial layer. As a whole, in top-down fabrication of cantilevers and bridges with nanometer scales by surface micromachining, release of the structures is performed by the sacrificial layer etching underneath with generation of the overhanging of the cantilever clamping [1–11, 16–19]. This overhanging can affect the mechanical characteristics [19]. The out-of-plane resonance frequency may be shifted towards lower values because of the increase in the effective length of the cantilever, which decreases the spring constant. Meanwhile, it is probable that the overhanging lowers the quality factor value due to support loss through the flexible fixation of the cantilevers [20].

Another parameter to consider is the curved shape at the cantilever clamping point (see figure 5). Due to the limitation in precision of the lithography technique, the clamping point of the cantilevers has a curved shape with a radius of about 0.5 μm. Usually, in the case of such nanostructures defined by optical lithography, curvature on a corner of a structure is difficult to avoid. As the structures are miniaturized to nanometer scale, the clamping point curvatures become more dominant.

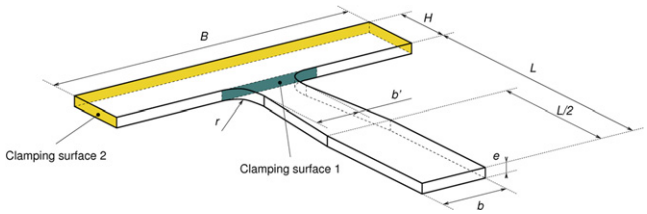

Figure 6. Geometry of the nanocantilever used in the finite-element simulations.

Recently, Ilic and coworkers mentioned that due to overhanging of the cantilever support, the resonance frequencies are lower than predicted by ideal beam theory [2, 3]. They found that the in-plane vibration is less sensitive to the overhanging. The same authors also demonstrated by experiment and simulation that, with the overhanging of the cantilever support, both the out-of-plane and in-plane resonance frequencies decrease as a function of the width [3].

5. Numerical simulations

In order to investigate how these non-ideal shapes mentioned above affect the resonance frequencies, simulations with the finite-element method were conducted for nanocantilevers with curvature at the clamping point and overhanging of the cantilever support. The finite-element code Cast3M, developed at CEA Saclay (France) [21], was used. The model geometry, shown in figure 6, is meshed with 21 651 ten-node tetrahedral elements. The mesh can be seen in figures 8 and 11. The numerical values of the geometrical parameters used in the simulations were $L = 14.3$ μm and $e = 340$ nm for the beam length and thickness, and an overhanging width $B = 42$ μm, large enough so that it had no noticeable influence on our numerical results. In addition to the non-ideal clamping shapes, it has been noticed that the cantilevers present a slight variation of the width between the apex and the clamping point: taking a closer look at figure 5, it can be seen that the width at the apex is slightly larger than at the end of the curved shape. To take this into account in the simulations, the beam's width was chosen as an affine function of the beam's axial coordinate in a region of length $L/2$ from the end of the curved shape (b' denotes the width at this point) and then constant and equal to b for the remaining part of the beam. In the simulations, the beam's widths b and b', the curvature radius at clamping point r and the overhanging depth H were varied.

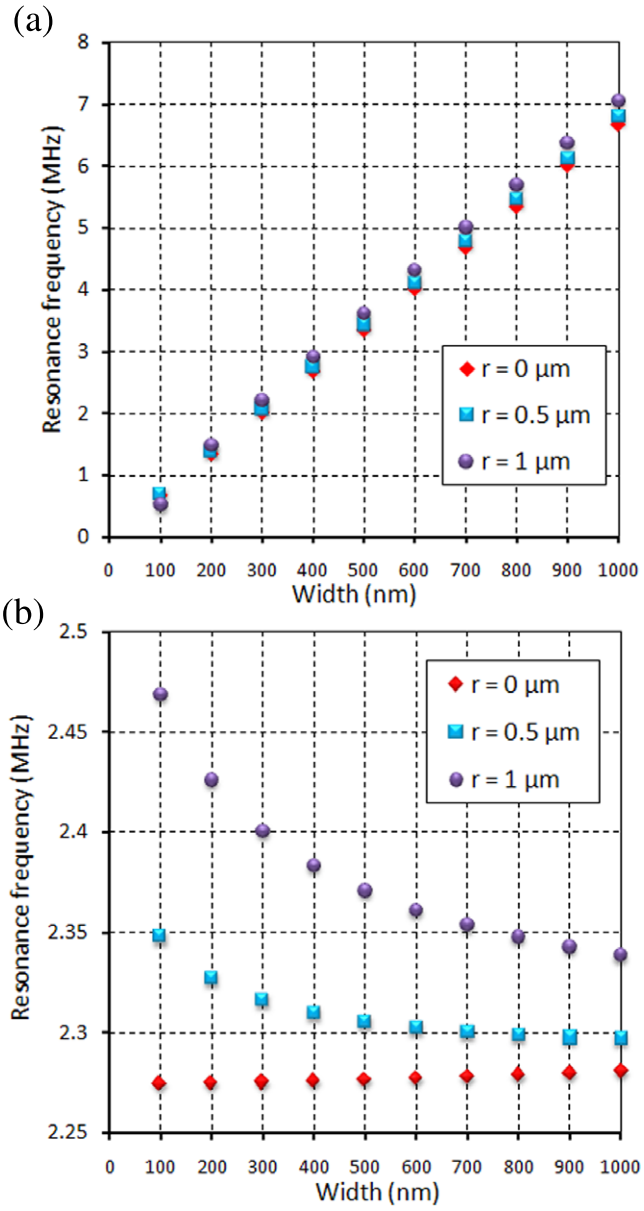

Figure 7. Simulation results of natural frequency evolution as a function of width, for various curvature radii at the clamping point ($r = 0$, 0.5, 1 μm) and a zero overhanging depth ($H = 0$). A uniform width is considered ($b = b'$). (a) In-plane mode, (b) out-of-plane mode.

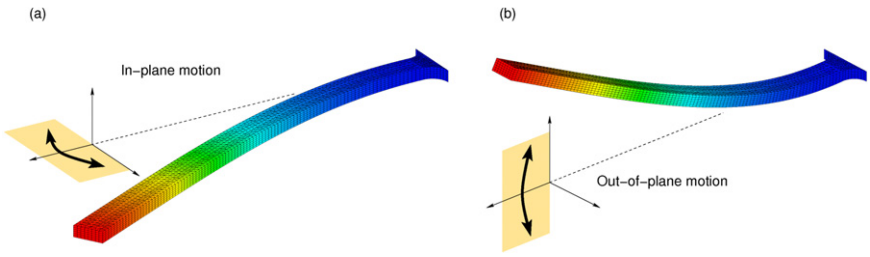

Figure 8. Mode shapes in the case of no overhanging depth ($H = 0$). The finite-element mesh is also shown. (a) In-plane mode shape, (b) out-of-plane mode shape.

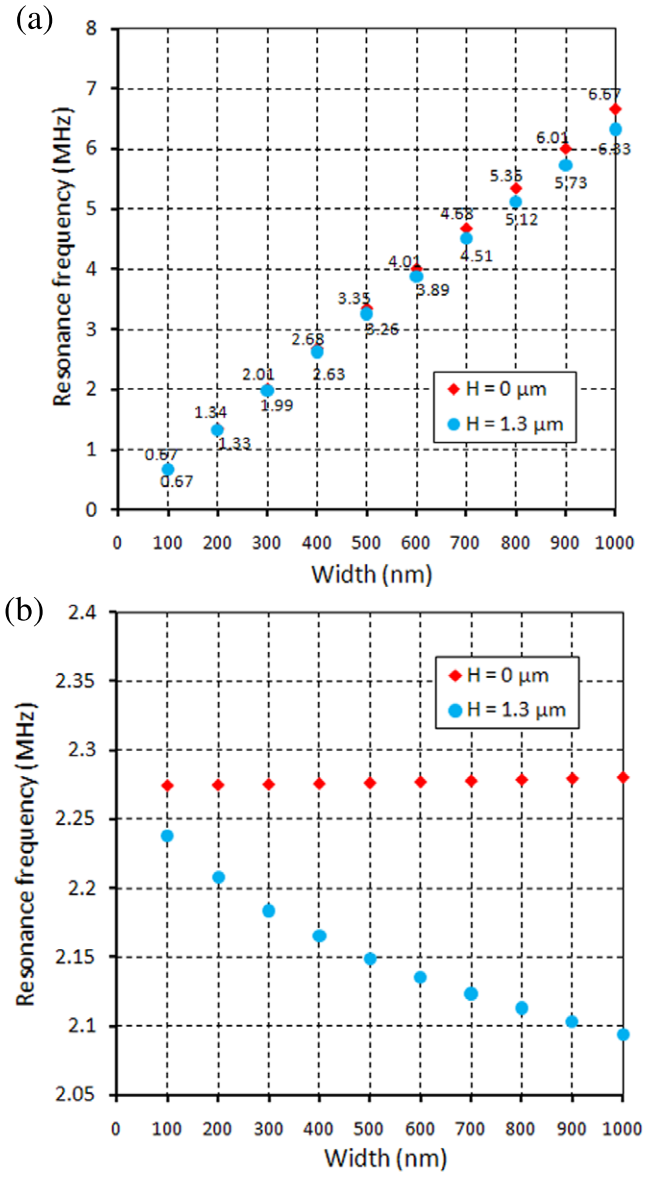

Figure 9. Simulation results of natural frequency evolution as a function of width, for various overhanging depths ($H = 0$ and 1.3 μm) and no curvature radius at the clamping point ($r = 0$). A uniform width is considered ($b = b'$). (a) In-plane mode, (b) out-of-plane mode.

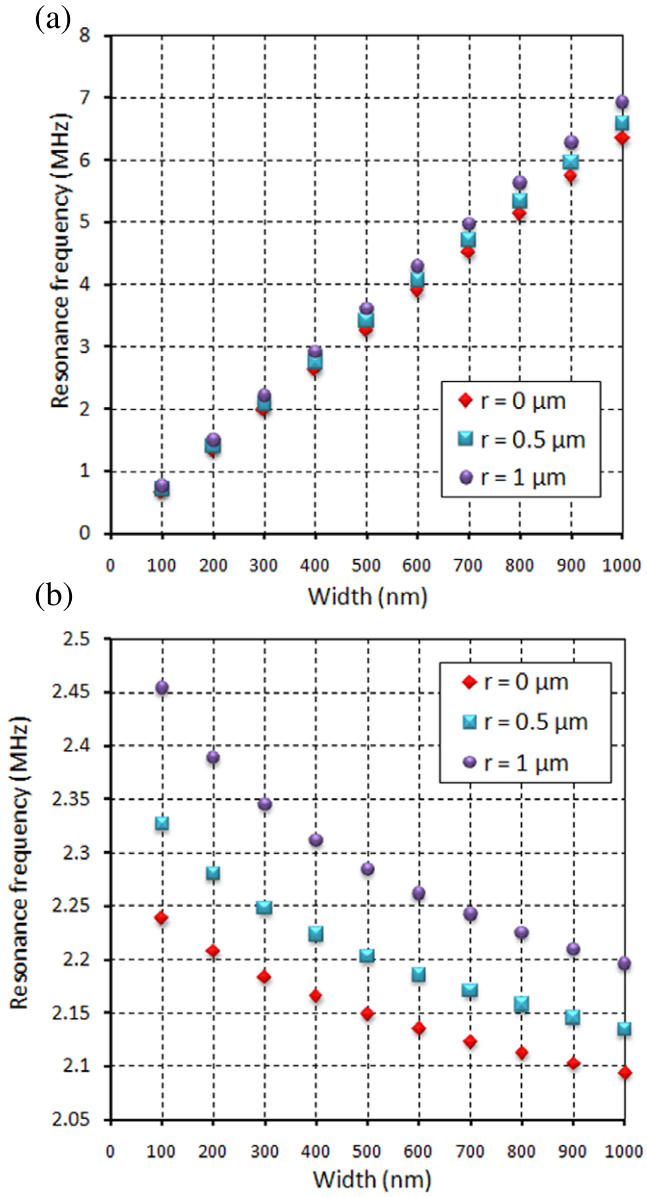

Figure 10. Simulation results of natural frequency evolution as a function of width, for various curvature radii at the clamping point ($r = 0$, 0.5, 1 μm) and an overhanging depth $H = 1.3$ μm. A uniform width is considered ($b = b'$). (a) In-plane mode, (b) out-of-plane mode.

The silicon used here for manufacturing the nanocantilevers was an anisotropic crystalline material [22]. As a consequence, one can expect that the mechanical properties of the nanocantilevers depend on the relative orientation of their neutral axis with respect to the crystal lattice. To evaluate the influence of the material as well as to identify the right choice for the material constants and model, we performed several simulations. The cantilever's neutral axis was oriented in the [110] direction of the silicon crystal lattice. In the first simulation, an orthotropic material was used. The material constants were those of a standard (100) silicon wafer with frame of reference [110], [$\bar{1}$10], [001], obtained in [22]: $E_x = E_y = 169$ GPa, $E_z = 130$ GPa, $\nu_{yz} = 0.36$, $\nu_{zx} = 0.28$, $\nu_{xy} = 0.064$, $G_{yz} = G_{zx} = 79.6$ GPa, $G_{xy} = 50.9$ GPa. In a second simulation, an isotropic material of Young's modulus $E = 169$ GPa (the one in the [110] direction), Poisson's ratio $\nu = 0.3$ and density $\rho = 2330$ kg m^{-1} was used. This was motivated by the fact that because the cantilevers are slender, the main deformation mechanism that governs their transverse oscillations is the compression/extension of the fibers in the [110] neutral axis direction, so that only the Young's modulus in this direction has an effect. Both simulations give the same results for the in-plane and out-of-plane natural frequencies with a deviation of less than 1.3%.

This result shows that an isotropic model with the right value of the Young's modulus is sufficient for simulations of transverse vibrations of silicon beam-like structures. However,

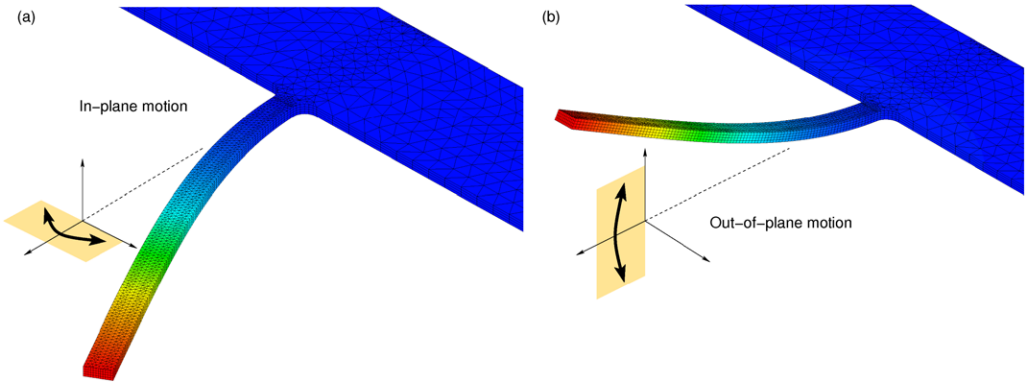

Figure 11. Mode shapes in the case of a non-zero overhanging depth. The finite-element mesh is also shown. (a) In-plane mode shape, (b) out-of-plane mode shape.

the following numerical results have been obtained with the orthotropic finite-element model, extremely easy to implement with the Cast3M software.

5.1. Effect of curvature at the clamping point of the cantilevers

Figure 7 shows the simulation results for the natural frequency evolution with respect to width and various values of curvature radius at the clamping point ($r = 0$, 0.5, 1 μm), with no overhanging depth ($H = 0$) and no width variation ($b' = b$). Figure 8 shows the corresponding mode shapes as well as the mesh of the finite-element model. Clamping surface 1 of figure 6 was then used as a boundary condition in the finite-element model. As the curvature radius at the clamping point becomes larger, the natural frequencies are increased both for the in-plane and out-of-plane motion. The main reason is the effective length, which decreases because of the curvature. In the out-of-plane mode, without curvature at the clamping point, the natural frequency is independent of the width as predicted by equation (1). Figure 7(b) shows that, in the case where the clamping point has curvature, the natural frequency of the out-of-plane mode can decrease with increasing width. Nevertheless, the widest cantilevers are less sensitive to the curvature at the clamping point in the sense that the out-of-plane natural frequency remains almost unchanged.

5.2. Effect of overhanging of the cantilever support

Simulation results for the natural frequency evolution as a function of the beam's width, for nanocantilevers without curvature at the clamping point ($r = 0$ μm) and no width variation ($b' = b$), are shown in figure 9 to evaluate the effect of a non-zero overhanging depth H ($H = 0$ and 1.3 μm are presented). Clamping surface 2 of figure 6 was then used as a boundary condition in the finite-element model. It shows that the natural frequencies decrease because of the overhanging both in the in-plane mode and in the out-of-plane mode. This trend is amplified by the increase of width [2, 3].

Figure 10 shows the simulation results combining both the effects of the overhanging depth ($H = 1.3$ μm) and various values of the curvature radius at the clamping point ($r = 0$, 0.5, 1 μm) on the evolution of the natural frequency as a function of the cantilever's width. The width is considered uniform ($b' = b$). It is found that, with increasing width, depending on the curvature radius, the natural frequencies are dramatically lower than those of figure 7, where the overhanging is not considered.

Finally, figure 12 shows simulation results for the natural frequency variation as a function of the overhanging depth for different cantilever widths, with a non-zero curvature radius at the clamping point (fixed at $r = 0.5$ μm) and a uniform width ($b = b'$). As the length of the overhanging increases, both the in-plane and the out-of-plane natural frequency decrease. The decrease in natural frequency with the overhanging length is more dominant in wider cantilevers.

5.3. Comparison with experiments

In figure 13, a comparison between simulation and experimental data for both the out-of-plane and in-plane modes' natural frequencies as a function of width is shown. The curvature radius at the clamping point was chosen as $r = 0.5$ μm and the overhanging depth of the cantilever's support was $H = 1.3$ μm; these values correspond to the reality of the fabricated nanostructures. To improve the match between theory and experiments, various slight variations of width between the clamping point and the apex were considered: $(b - b')/b = 0\%$, 4% and 8%. Those values roughly correspond to what can be estimated with the SEM images of figure 5. In the case of the in-plane mode (figure 13(a)), the resonance frequencies of the experimental results correspond rather well to the simulation results. In the case of the out-of-plane mode (figure 13(b)), the decrease rate in the natural frequencies as a function of width is higher in the measured results and the measured frequency values are smaller than the theoretical ones. Considering the imperfect clamping point (non-zero radius of curvature and overhanging depth) leads to a good trend of the natural frequencies that decrease as a function of width, but an error of about 10% on average remains. Then, adding to those imperfections a non-uniform width improves the simulations by reducing the error to about 5% on average.

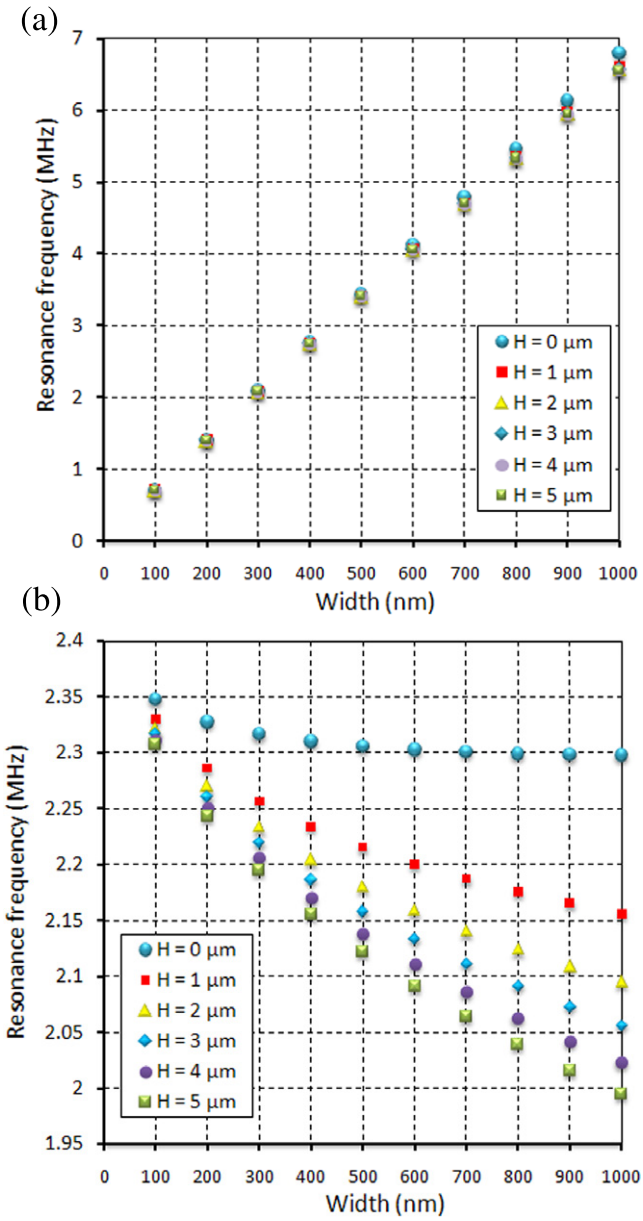

Figure 12. Simulation results of natural frequency evolution as a function of width, for various overhanging depths ($H = 0$, 1, 2, 3, 4, 5 μm) and a fixed curvature radius at the clamping point, $r = 0.5$ μm. A uniform width is considered ($b = b'$). (a) In-plane mode, (b) out-of-plane mode.

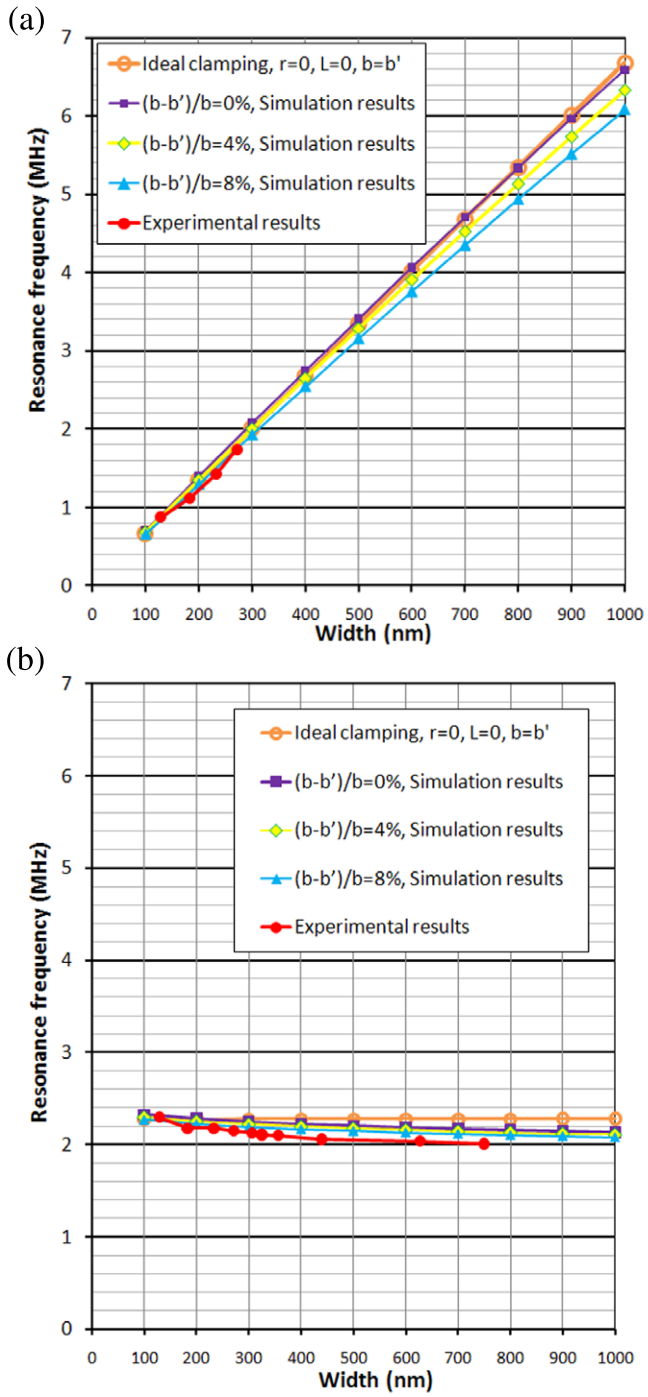

Figure 13. Comparison between experimental and simulation results for the natural frequency evolution as a function of width, with curvature radius at clamping point $r = 0.5$ μm and with overhanging depth of the cantilever support $H = 1.3$ μm. Various width variations along the beam's length have been considered ($(b - b')/b = 0\%$, 4% and 8%). (a) In-plane mode, (b) out-of-plane mode.

6. Conclusion

We fabricated silicon nanocantilevers with a smallest width of 100 nm by stepper UV lithography. To measure their vibratory characteristics, the nanocantilevers were excited by electrostatic force by approaching a tungsten tip inside an SEM. Their fundamental resonance frequencies, in directions both parallel to the wafer plane (in-plane mode) and orthogonal to the wafer plane (out-of-plane mode) were detected visually with the SEM and compared to theoretical and numerical results. Slight decreases in resonance frequencies as a function of nanocantilever width, for the out-of-plane mode, were observed. By considering various finite-element models, it is shown that this is mainly due to various geometrical imperfections of the cantilevers: a curved shape, an overhanging at the clamping point as well as non-uniform width along the axial coordinate.

Acknowledgments

The French National Agency for Research (program ANR/PNANO 2008, project NEMSPIEZO 'ANR-08-NANO-015') is gratefully acknowledged for financial support.

References

[1] Craighead H G 2000 Nanoelectromechanical systems *Science* **290** 1532–5
[2] Ilic B, Krylov S, Kondratovich M and Craighead H G 2007 Selective vibrational detachment of microspheres using optically excited in-plane motion of nanomechanical beams *Nano Lett.* **7** 2171–7
[3] Ilic B, Krylov S and Craighead H G 2010 Young's modulus and density measurements of thin atomic layer deposited films using resonant nanomechanics *J. Appl. Phys.* **108** 044317
[4] Ilic B, Krylov S, Aubin K, Reichenbach R and Craighead H G 2005 Optical excitation of nanoelectromechanical oscillators *Appl. Phys. Lett.* **86** 193114
[5] Ilic B, Yang Y, Aubin K, Reichenbach R, Krylov S and Craighead H G 2005 Enumeration of DNA molecules bound to a nanomechanical oscillator *Nano Lett.* **5** 925–9
[6] Carr D W, Sekaric L and Craighead H G 1998 Measurement of nanomechanical resonant structures in single-crystal silicon *J. Vac. Sci. Technol.* B **16** 3821
[7] Carr D W and Craighead H G 1997 Fabrication of nanoelectromechanical systems in single crystal silicon using silicon on insulator substrates and electron beam lithography *J. Vac. Sci. Technol.* B **15** 2760
[8] Ilic B, Krylov S, Bellan L M and Craighead H G 2007 Dynamic characterization of nanoelectromechanical oscillators by atomic force microscopy *J. Appl. Phys.* **101** 044308
[9] Zalalutdinov M, Ilic B, Czaplewski D, Zehnder A, Craighead H G and Parpia J M 2000 Frequency-tunable micromechanical oscillator *Appl. Phys. Lett.* **77** 3287
[10] Masmanidis S C, Karabalin R B, De Vlaminck I, Borghs G, Freeman M R and Roukes M L 2007 Multifunctional nanomechanical systems via tunably coupled piezoelectric actuation *Science* **317** 780–3
[11] Li M, Tang H X and Rouke M L 2007 Ultra-sensitive NEMS-based cantilevers for sensing, scanned probe and very high-frequency applications *Nat. Nanotechnol.* **2** 114–20
[12] Perisanu S, Gouttenoire V, Vincent P, Ayari A, Choueib M, Bechelany M, Cornu D and Purcell S T 2008 Mechanical properties of SiC nanowires determined by scanning electron and field emission microscopies *Phys. Rev.* B **77** 165434
[13] Vincent P, Perisanu S, Ayari A, Choueib M, Gouttenoire V, Bechelany M, Brioude A, Cornu D and Purcell S T 2007 Driving self-sustained vibrations of nanowires with a constant electron beam *Phys. Rev.* B **76** 085435
[14] Ayari A, Vincent P, Perisanu S, Choueib M, Gouttenoire V, Bechelany M, Cornu D and Purcell S T 2007 Self-oscillations in field emission nanowire mechanical resonators: a nanometric DC–AC conversion *Nano Lett.* **7** 2252–7
[15] Poncharal P, Wang Z L, Ugarte D and de Heer W A 1999 Electrostatic deflections and electromechanical resonances of carbon nanotubes *Science* **283** 1513–6
[16] Davis Z J, Abadal G, Kuhn O, Hansen O, Grey F and Boisen A 2000 Fabrication and characterization of nanoresonating devices for mass detection *J. Vac. Sci. Technol.* B **18** 612–6
[17] Davis Z J *et al* 2003 Monolithic integration of mass sensing nano-cantilevers with CMOS circuitry *Sensors Actuators* A **105** 311–9
[18] Teva J, Abadal G, Davis Z J, Verd J, Borrisé X and Boisen A Pérez-Murano F and Barniol N 2004 On the electromechanical modelling of a resonating nano-cantilever-based transducer *Ultramicroscopy* **100** 225–32
[19] Gavan K B, van der Drift E W J M, Venstra W J, Zuiddam M R and van der Zant H S J 2009 Effect of undercut on the resonant behaviour of silicon nitride cantilevers *J. Micromech. Microeng.* **19** 035003
[20] Yang J L, Ono T and Esashi M 2002 Energy dissipation in submicrometer thick single-crystal silicon cantilevers *J. Microelectromech. Syst.* **11** 775–83
[21] Verpeaux P, Charras T and Millard A 1988 Castem 2000: une approche moderne du calcul des structures *Calcul des Structures et Intelligence Artificielle* (Paris: Pluralis) pp 261–71
[22] Hopcroft M A, Nix W D and Kenny T W 2010 What is the Young's modulus of silicon? *J. Microelectromech. Syst.* **19** 229–38